A Multi-Plane Augmented Reality Head-Up Display System Based on Volume Holographic Optical Elements With Large Area

Zhenlv Lv, Juan Liu, and Liangfa Xu

***Abstract*—The traditional head-up display (HUD) system has the disadvantages of a small area and a single display plane, here we propose and design an augmented reality (AR) HUD system with multi-plane, large area, high diffraction efficiency and a single picture generation unit (PGU) based on holographic optical elements (HOEs). Since volume HOEs have excellent angle selectivity and wavelength selectivity, HOEs of different wavelengths can be designed to display images in different planes. Experimental and simulated results verify the feasibility of this method. Experimental results show that the diffraction efficiencies of the red, green and blue HOEs are 75.2%, 73.1% and 67.5%. And the size of HOEs is 20 cm × 15 cm. Moreover, the three HOEs of red, green and blue display images at different depths of 150 cm, 500 cm and 1000 cm, respectively. In addition, the field of view (FOV) and eye-box (EB) of the system are 12° × 10° and 9.5 cm × 11.2 cm. Furthermore, the light transmittance of the system has reached 60%. It is believed that this technique can be applied to the augmented reality navigation display of vehicles and aviation.**

***Index Terms*—Holography, diffractive imaging, imaging systems.**

I. Introduction

THE vehicle head-up display (HUD) system can display driving information such as vehicle speed, fuel consumption, warning signals and navigation arrows to the driver through the windshield or combiner [1]–[4]. With HUD, the driver always looks straight ahead on the road without frequently moving the sight to see the dashboard, thus improving driving safety [5].

The traditional HUD provides vehicle information on a certain depth plane through a small area combiner, without fusion and interaction with the external real environment. However, an augmented reality (AR) HUD can provide richer information to the driver at different depth planes, such as navigation information at a long distance, warning signals at a medium distance, and basic information at a short distance. Compared with traditional HUD, AR HUD can greatly improve the driving experience and safety by providing interactive information, which is expected to have a huge automotive and aviation application market.

Manuscript received June 22, 2021; revised August 4, 2021; accepted August 13, 2021. Date of publication August 18, 2021; date of current version September 17, 2021. This work was supported by the National Natural Science Foundation of China under Grants 61975014 and 62035003. *(Corresponding author: Juan Liu.)*

The authors are with the Beijing Engineering Research Center for Mixed Reality and Advanced Display, School of Optics and Photonics, Beijing Institute of Technology, Beijing 100081, China (e-mail: 3120195305@bit.edu.cn; juanliu@bit.edu.cn; 1483883724@qq.com).

Digital Object Identifier 10.1109/JPHOT.2021.3105670

The research objective of AR HUD is to provide multiple virtual images with different projection distances for the driver. The technical solutions to realize multi-plane display mainly include geometric optics [6]–[8], dynamic varifocal components [9]–[12], digital holography [13]–[17] and volume holography [18]. A HUD with multiple picture generation units (PGUs) and multiple combiners using geometric optics is expensive and bulky, and it is difficult to integrate in the limited space below the dashboard [13], [14]. The structure of the HUD with one PGU and one combiner is relatively compact, but the use of free-form surface mirror increases the difficulty of system design and processing [15]. Using dynamic varifocal components, such as liquid lenses [9], Pancharatnam–Berry lenses [10], and multilayer polymer switchable liquid crystals [11], is another potential solution for AR HUD, which has been discussed a lot in AR near-eye display [12]. However, compared with the near-eye display, due to the need for a larger eye-box (EB), the size of the optical components in the HUD is much larger. Therefore, high quality, large size and high varifocal speed are the main limiting factors for the application of dynamic components to HUD. Digital holography can realize multi-plane display by calculating and loading holograms of different depths, but it has the problems of low resolution, slow calculation speed and difficulty in color display [17]. In addition, volume holography can also be used for multi-depth plane display. The volume holographic optical elements (HOEs) have great wavelength selectivity and angle selectivity [19], which can avoid the crosstalk between the reflected image and the diffracted image. A dual-focal-plane volume holographic HUD that combines a wavelength multiplexing HOE with two PGUs is proposed [18]. The prototype is relatively bulky due to the use of two PGUs. Moreover, the display image is difficult to distinguish in sunlight because of low diffraction efficiency, and there are problems with image distortion and color shift.

In this paper, we propose an AR HUD system with multi-plane, large area, high diffraction efficiency, and a single PGU based on the wavelength selectivity, angle selectivity and imaging function of volume HOEs.

II. Basic Idea and Principle

The basic structure diagram of the multi-plane AR HUD system is shown in Fig. 1. The system is mainly composed of three parts: laser projection module, diffuser and holographic combiner. With the characteristics of miniaturization, high

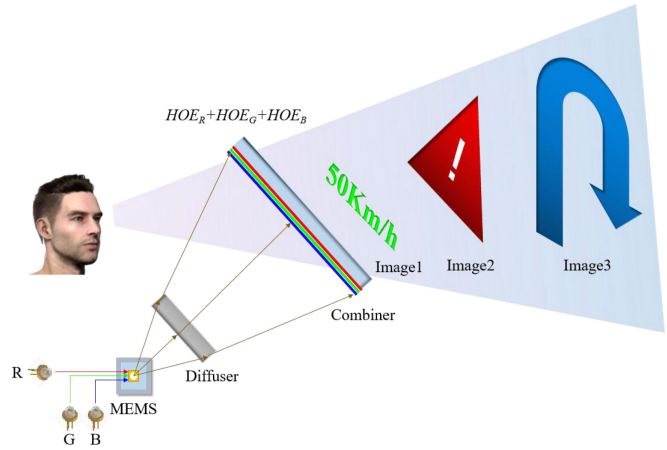

Fig. 1. Schematic diagram of the proposed multi-plane holographic head-up display system.

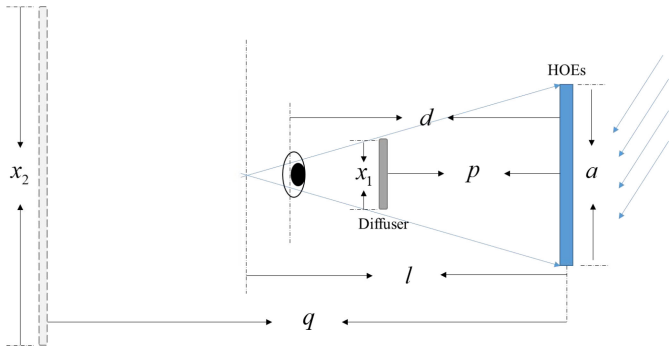

Fig. 2. Diagram of the relationship between object and virtual image.

brightness and clear imaging at any distance, the laser projection module including Micro-Electro-Mechanical System (MEMS) mirror, optical engine and controller is used to generate the target image. The diffuser receives the image sent by the projection module and is used as the object plane for HOE imaging. The holographic combiner composed of a glass substrate and HOEs with three different wavelengths of red, green and blue is used as the imaging element. HOEs of different wavelengths correspond to different imaging depths to realize multi-plane display.

III. Parameter Design and Numerical Simulation

A. Parameter Design

It is necessary to analyze the relationship between objects and images when the HUD system proposed in this paper is used as an imaging system. When analyzing the imaging characteristics of HOEs, the diffuser screen is equivalent to the object plane. The object-image relationship of the system is shown in Fig. 2.

The image displayed by the HUD system is an enlarged virtual image, so there is the following relationship between the object and the image:

$$\frac{1}{p} - \frac{1}{q} = \frac{1}{f} \tag{1}$$

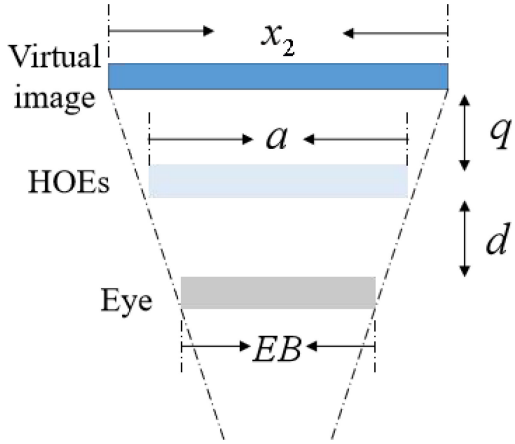

Fig. 3. The relationship between virtual image, HOEs and human eye.

Where the p, q and f are the object distance, image distance and focal length of the system, respectively.

The magnification M between the virtual image and the real image is as follows:

$$M = q/p \tag{2}$$

So the virtual image size x_2 is:

$$x_2 = M \times x_1 \tag{3}$$

Where x_1 is the size of the image projected on the diffuser.

When used as an imaging element, the reflective volume HOEs can achieve a transmissive display of different planes through the combination of the virtual image imaging function and the reflective function. The virtual image distance during actual observation is the distance between the human eye and the HOEs plus the virtual image distance of the system. Therefore, the field of view (FOV) of the system is as follows:

$$FOV = 2\arctan\left[\frac{x_2}{2\,(q+d)}\right] \tag{4}$$

Where d is the distance between the human eye and the HOEs.

EB is one of the key indicators of the HUD system. HUD requires a larger eye movement range than HMD. According to the relationship between virtual image, HOEs and human eye, as shown in Fig. 3, the EB of the system can be expressed as:

$$EB = a - (x_2 - a) \times d/q \tag{5}$$

The EB and the FOV have the following relationships:

$$EB = a - 2\tan\left(FOV/2\right) \times d \tag{6}$$

It can be seen from the above formula that when the size of HOEs is constant, there is a negative correlation between FOV and EB. Therefore, the way to ensure that the system has proper FOV and EB at the same time is to increase the size of HOEs, but it will increase the difficulty of design and production.

The recording and reconstruction principles of the multi-plane AR HUD system are shown in Fig. 4. The OR, OG and OB are the convergence points of the object light waves corresponding to

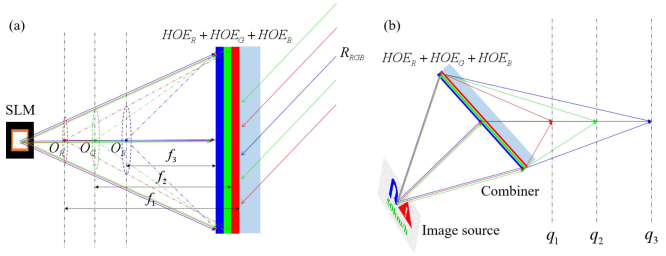

Fig. 4. (a) The recording principle of the system proposed in this paper. (b) The reconstruction principle of the system proposed in this paper.

TABLE I
THE DESIGN PARAMETERS OF HOE_R, HOE_G AND HOE_B

	HOE_R	HOE_G	HOE_B
p(cm)	30	30	30
q(cm)	150	500	1000
f(cm)	37.5	31.91	30.93
Size(cm×cm)	20×15	20×15	20×15
d(cm)	50	50	50

three different wavelengths modulated by spatial light modulator (SLM). f_1, f_2 and f_3 are the equivalent focal lengths of the HOEs corresponding to the three wavelengths of red, green and blue. q_1, q_2 and q_3 are the virtual image distances of the red, green and blue HOEs at the same object distance.

During recording, the three-wavelength object light waves modulated by the SLM are equivalent to spherical light waves with different degrees of convergence, as shown by the dotted line in the Fig. 4(a). The reference light waves are all parallel light waves. Therefore, the red, green, and blue HOEs as imaging elements have different diopters. During reconstruction, the distances between the target points on the diffuser and the HOEs are constant as shown in the Fig. 4(b), that is, the object distances of the three-wavelength HOEs are the same. For the entire system, the HOEs of the three wavelengths have the same object distances and different focal lengths, thus multi-plane displays with different image distances can be realized.

The design parameters of HOE_R, HOE_G and HOE_B are shown in Table I. The distance between the diffuser and the HOEs is constant at 30 cm. The focal lengths of HOE_R, HOE_G and HOE_B are 37.5 cm, 31.91 cm and 30.93 cm respectively. The virtual image distances of HOE_R, HOE_G and HOE_B are 150 cm, 500 cm and 1000 cm respectively. The sizes of the three HOEs are all 20 cm × 15 cm. The distance between the human eye and the HOEs is 50 cm. In addition, the size of the diffuser is 10 cm × 10 cm. The angle between the reference light and the normal direction of the holographic recording plane is 45°.

B. Numerical Simulation

Based on the designed parameters, we carry out numerical simulation to verify the method proposed in this paper. The simulation process consists of three steps: The first step is the diffraction in the free space between the diffuser and the HOEs. The second step is to superimpose the phase factor of the HOEs.

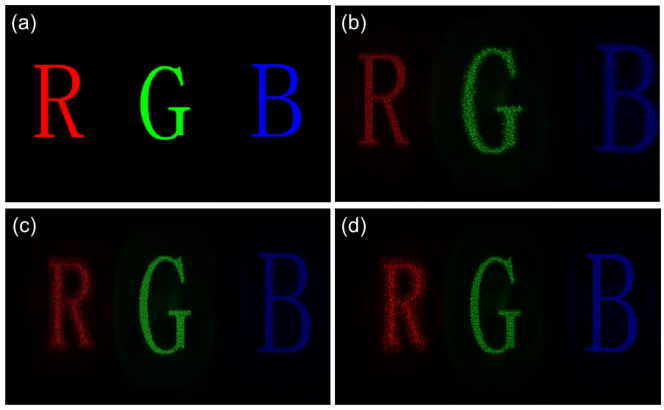

Fig. 5. (a) Input image. (b) Focus on the letter R at 150 cm. (c) Focus on the letter G at 500 cm. (d) Focus on the letter B at 1000 cm.

The third step is the diffraction of the free space between the HOEs and the virtual image plane.

The calculation of diffraction in free space is based on Kirchhoff's diffraction integral formula, as shown below:

$$E(x,y) = K \int\int A(\xi,\eta) \frac{\exp(jkr)}{r} d\xi d\eta \tag{7}$$

Where ξ and η are the coordinates of the diffractive aperture plane, K is the complex constant, k is the wave vector, and r is the distance from the target point to the center of the spherical wave.

In addition, since the reference light is incident obliquely, the phase factor of the HOEs is as follows:

$$\phi = -k\sqrt{x^2 + y^2 + {r_0}^2} + kx \sin\theta \tag{8}$$

Where x and y are the coordinates of the HOE plane, r_0 is the distance from the convergence point of the spherical wave to the HOE, and θ is the angle of the reference beam deviating from the axis.

The numerical simulation results are shown in Fig. 5. The input image is the three colored letters containing R, G and B loaded on the diffuser. When the observation plane is 150 cm away from HOEs, the letter R is clear and the letters G and B are blurred. When the observation plane is 500 cm away from HOEs, the letter G is clear and the letters R and B are blurred. When the observation plane is 1000 cm away from HOEs, the letter B is clear and the letters R and G are blurred.

Therefore, the simulation results prove the feasibility of the method in this paper. However, it can be seen from the simulation results that the displayed image is extended in the vertical direction and the image quality is degraded compared to the input image. The asymmetrically recorded planar HOEs have vertical astigmatism, horizontal coma aberration, and defocus aberration. And the aberrations increase as the incident angle deviates from the Bragg matching angle. Therefore, the HOEs should meet the Bragg matching condition during reconstruction to improve the imaging quality of the HUD system. However, the consistency of the incident angle and the Bragg angle cannot completely eliminate the aberrations caused by the off-axis recording.

The formula for the primary aberration W of HOEs is as follows:

$$\mathrm{W} = -\frac{\left(x^2+y^2\right)^2}{8}S + \frac{x^2+y^2}{2}\left(C_x x + C_y y\right) + \frac{1}{2}\left(A_x x^2 - 2A_{xy}xy + A_y y^2\right) \tag{9}$$

Where the first term is spherical aberration, the second term is coma, and the third term is astigmatism. The expressions of the coefficients in the above formula are as follows:

$$\mathrm{S} = \frac{1}{l_c^3} - \frac{1}{l_I^3} + \left(\frac{1}{l_O^3} - \frac{1}{l_R^3}\right) \tag{10}$$

$$\begin{cases} C_x = \frac{x_c}{l_c^3} - \frac{x_I}{l_I^3} + \left(\frac{x_O}{l_O^3} - \frac{x_R}{l_R^3}\right) \\ C_y = \frac{y_c}{l_c^3} - \frac{y_I}{l_I^3} + \left(\frac{y_O}{l_O^3} - \frac{y_R}{l_R^3}\right) \end{cases} \tag{11}$$

$$\begin{cases} A_x = \frac{x_c^2}{l_c^3} - \frac{x_I^2}{l_I^3} + \left(\frac{x_O^2}{l_O^3} - \frac{x_R^2}{l_R^3}\right) \\ A_{xy} = \frac{x_c y_c}{l_c^3} - \frac{x_I y_I}{l_I^3} + \left(\frac{x_O y_O}{l_O^3} - \frac{x_R y_R}{l_R^3}\right) \\ A_y = \frac{y_c^2}{l_c^3} - \frac{y_I^2}{l_I^3} + \left(\frac{y_O^2}{l_O^3} - \frac{y_R^2}{l_R^3}\right) \end{cases} \tag{12}$$

Where x and y are the coordinates of the object point and the image point in the x-y plane. l is the distance from the object point or image point to the origin of the coordinate. The subscripts O and R indicate the object light wave and reference light wave during recording. The subscripts C and I indicate the object light wave and image light wave during reconstruction.

It can be seen from the above formulas that the longer the distance between the object point and the origin of the coordinates will result in serious aberrations. For the multi-plane HUD system in this paper, the adjustment of the field of view angle is achieved by changing the size of the object, under the premise that the recording parameters of the HOEs are fixed. Therefore, the reduction of FOV or object size can reduce aberrations of the system. In addition, feasible methods to further correct astigmatism include adding a cylindrical mirror to the recording optical path and fabricating HOEs on a curved glass substrate [20], [21].

IV. Experimental Verification

Based on the theoretically designed parameters, we record the HOEs corresponding to the three depth planes by the holographic interference exposure method. $\mathrm{HOE_R}$, $\mathrm{HOE_G}$ and $\mathrm{HOE_B}$ are exposed independently and stacked on a same glass substrate in layers to achieve higher diffraction efficiency. The principle diagram of the recording optical path is shown in Fig. 6.

The green laser is a Genesis CX SLM with a power of 5w from Coherent. The red and blue lasers are single longitudinal mode lasers with a power of 400mw from Changchun New Industry Co., Ltd. And the holographic recording material is Bayfol HX200. $\mathrm{HWP_1}$ is used to adjust the splitting ratio of the system. $\mathrm{HWP_2}$ is used to make the polarization of the reference light and the object light the same. $\mathrm{L_2}$ is used to generate a large-area parallel beam with a diameter of 30 cm. In the 4f system, $\mathrm{L_3}$ is an achromatic doublet lens with a focal length of 75 mm and a diameter of 2 inches, and $\mathrm{L_4}$ is a freeform lens with a focal length of 30 mm and a diameter of 50 mm. Due to the lower power of the red and blue lasers, the exposure time is about six minutes. To ensure the stability during the exposure process, we use the Newport's vibration control experimental platform and a large-size frame for fixing the recording material.

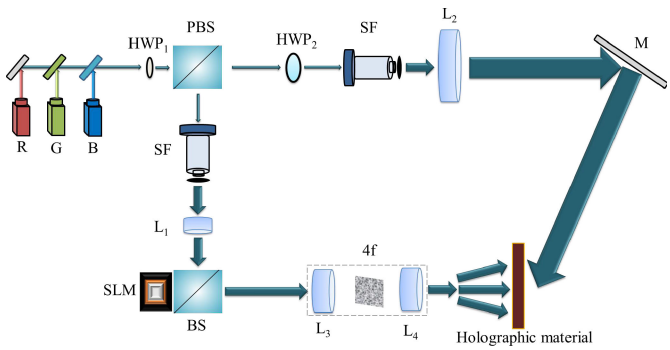

Fig. 6. The principle diagram of the recording optical path.

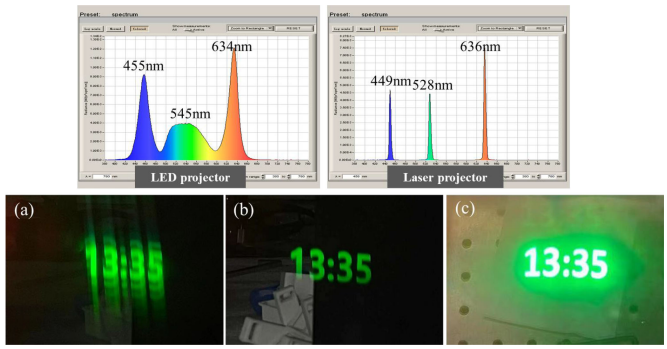

Fig. 7. The spectra and display effects of the LED projector and the laser projector. (a) and (b) are the display effects with and without filter when the LED projector is used as the image source. (c) is the display effect when the laser projector is used as the image source.

The aberrations are mainly introduced by the light source of the HUD system. So we test the display effects of LED projector and laser projector as the light source of HUD system respectively. The spectra of the LED projector and laser projector are shown in the Fig. 7. Due to the large spectral width of the LED projector, there are obvious chromatic aberrations in the reconstructed images, as shown in Fig. 7(a). We reduce the chromatic aberration by introducing filters, but it will lead to a decline in light energy utilization, as shown in Fig. 7(b).

Because of the narrow spectral width of the laser projector, there is no obvious chromatic aberration in the experiment. In addition, laser projector has higher brightness than LED projector, as shown in the Fig. 7(c). Therefore, we choose to use a laser projector as the image source of the system. The main factor that affects the image quality of the HUD system with the laser projector as the light source is laser speckle.

The prototype of the multi-plane AR HUD system consists of three parts: a laser projector, a diffuser and three-layer HOEs, as shown in Fig. 8(a). The light source is a miniature laser projector manufactured by Ultimems, with a resolution of 1280

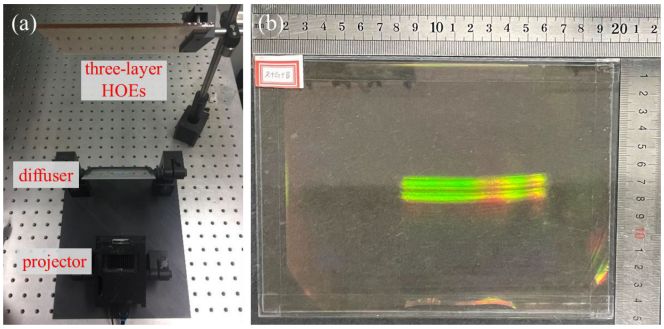

Fig. 8. (a) The prototype of the multi-depth holographic HUD system. (b) the fabricated three-layer HOEs with a size of 20 cm × 15 cm.

Fig. 9. (a), (b) and (c) are the display effects when the camera focuses on the three letters R, G and B at different distances.

× 760, a brightness of 30 lm, and a horizontal divergence angle of 43.15°. The diffuser is DG100 × 100-1500 from Thorlabs. Three layers of monochromatic holographic films are stacked on the same glass substrate with a thickness of 2 mm using a vacuum bonding method to achieve the effect of lightness and high light transmission. The actual fabricated three-layer HOEs with a size of 20 cm × 15 cm are shown in Fig. 8(b), and the strip pattern is the diffraction image under the LED fluorescent tube.

The multi-plane display effect of the prototype has been verified by experiments. Three letters of the same size including R, G, and B are the original input image. The display effects observed by the camera 50 cm away from the HOEs are shown in Fig. 9. When the camera focuses on the letter R at 1.5m, the other two letters G and B are blurred. When the camera focuses on the letter G at 5m, the other two letters R and B are blurred. When the camera focuses on the letter B at 10m, the other two letters R and G are blurred. In addition, the magnifications of the three letters are different due to the different imaging distances. The letter R and the letter B correspond to the minimum and maximum magnification respectively. Free-form lenses and achromatic doublet lenses are used in the optical path on the side of the signal light to reduce the modulation error of different wavelengths in the exposure. However, due to the shrinkage characteristics of the recording material and the contingency of the post-processing process, there is still a little deviation between the experimental value and the theoretical value of the focal length. When the deviation is reflected in the actual display of the HUD, the imaging planes corresponding to the different wavelengths will be in an interval value instead of a definite value. Although the depth of the imaging plane of each wavelength is not a certain value, the imaging planes of three different wavelengths are still not at the same depth, so the actual driving experience of the driver is not affected.

Fig. 10. The AR display effect of the multi-plane holographic HUD system.

The AR display effect of the HUD system in car navigation is shown in Fig. 10. The near field of vision displays basic information such as vehicle speed and time through the green HOE. The far field of vision displays the navigation information of road fusion through the blue HOE. In addition, auxiliary information such as warning signs can also be displayed through the red HOE. It can be seen from Fig. 8 that the resolution of the generated image is not very high. The reason for this phenomenon is that the diffuser in the projection module of the system serves as the object plane for HOE imaging. We test the imaging quality of the diffuser with different grit of 120, 220, 600 and 1500, and the results show that the imaging resolution of the diffuser with 1500 grit was relatively the highest. In the experiment, we use a diffuser with 1500 grit as the object surface for imaging.

Equation (6) shows that there is a negative correlation between FOV and EB. Therefore, we reduce the FOV and increase the EB at the same time by reducing the size of the object plane. The final FOV and EB of the system are 12° × 10° and 9.5 cm × 11.2 cm, respectively. In addition, the EB can be further expanded by producing a larger size HOE. It is worth mentioning that the aberration can be further reduced by increasing the size of the HOEs. Because increasing the size of the HOEs is equivalent to increasing the aperture of the imaging lens of the system.

V. Analysis of Results

A. *Diffraction Efficiency*

For the AR HUD display, too dark navigation signals will be inconvenient for the driver to observe, and too bright signals will affect the driver's judgment of the actual road conditions. Therefore, we analyze the diffraction efficiencies of different gratings. The processing methods used for multi-plane HOEs include three-layer stacking and single-layer multiplexing. Compared with three-layer stacking, it is difficult for the single-layer multiplexed HOEs to adjust the diffraction efficiencies of HOEs with three different wavelengths. Moreover, due to the large size

TABLE II
RECORDING WAVELENGTH AND RECONSTRUCTION WAVELENGTH OF HOE_R, HOE_G AND HOE_B

	recording	reconstruction
Red	639nm	636nm
Green	532nm	528nm
Blue	457nm	449nm

of the HOEs, holographic multiplexing will cause the uniformity of the grating to decrease. Therefore, we choose the three-layer stacking method to record HOEs. The three wavelengths of the laser used to record the HOEs are 639 nm, 532 nm and 457 nm. The three peak wavelengths of the laser projector used for display measured by the spectrometer are 636 nm, 528 nm and 449 nm. The data are shown in Table II. Since the recording wavelength and the reconstruction wavelength are not the same, the Bragg mismatch will cause the diffraction efficiency to decrease. Moreover, the greater the wavelength shift, the greater the loss of diffraction efficiency. Therefore, the diffraction efficiency of the three-wavelength HOEs decreases in order of red, green and blue.

A solution to this problem is to use angular offset to compensate for wavelength offset to ensure that Bragg matching conditions are still met when the reconstructed wavelength is inconsistent with the recorded wavelength [22], [23]. The relationship between the Bragg mismatch parameter δ and the angular offset $\Delta\theta$ and the wavelength offset $\Delta\lambda$ is as follows:

$$\delta = \Delta\theta k \sin(\varphi - \theta_0) - \Delta\lambda k^2/4\pi n_0 \tag{13}$$

Where k is the wave vector, θ_0 is the incident angle of the reference light during recording, φ is the tilt angle of grating vector, n_0 is the bulk index of refraction of the material.

It can be seen from the above formula that the Bragg mismatch parameter can be guaranteed to be zero by simultaneously changing the values of the wavelength offset and the angle offset. In addition, when the diffraction efficiency of the grating is fixed, the intensity of the signal light can be changed by adjusting the brightness of the laser projector.

Limited by the stability of the recording platform, the characteristics of the material, the accuracy of the optical components, etc., compared with the small-sized HOEs, the large-sized HOEs have the problem of uneven diffraction efficiency distribution. We redefine the diffraction efficiency of the HOEs to better reflect the uniformity and diffraction efficiency of the large-size HOEs recorded in the experiment. We divide the display image into 24 areas, 8 in the horizontal direction and 3 in the vertical direction, as shown in Fig. 11. First calculate the diffraction efficiency of the i-th area η_i, η_i is the average of the diffraction efficiencies of ten random positions in each region. Then the actual diffraction efficiency η is the average of the diffraction efficiencies of N areas.

$$\eta = \frac{\sum_{i=1}^{N} \eta_i}{N} = \frac{\sum_{i=1}^{N} \left(\frac{\sum_{k=1}^{10} I_{Dki}}{I_0} \right)}{N} \tag{14}$$

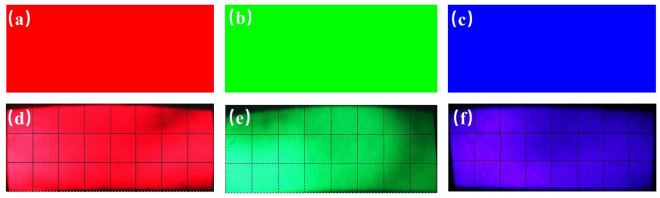

Fig. 11. (a)-(c) Loaded image of red, green and blue HOEs. (d)-(f) Displayed image of red, green and blue HOEs.

TABLE III
EXPERIMENTAL DATA OF LIGHT TRANSMITTANCE UNDER DIFFERENT CONDITIONS

	Glass substrate	Single layer HOE	Glass substrate + Three-layer HOEs	Glass substrate + Three-layer HOEs (one month later)
Transmittance	90%	88%	56%	60%

Where N is the number of areas, and η_i is the diffraction efficiency of the i-th area, I_0 is the input light intensity, and I_{Dki} is the diffracted light intensity of the k-th point in the i-th area.

The average diffraction efficiencies of the red, green and blue HOEs measured in the experiment are 75.2%, 73.1% and 67.5%.

B. Transmittance

We also analyze the transmittance of the system, because the transmittance of the HUD is a key parameter in the field of navigation display. With the increase of exposure, the holographic material gradually changes from dark purple to lighter color. Since the exposure dosage during the recording of the HOEs does not reach the maximum recording dosage of the holographic material, the transmittance of the HOEs after recording will increase under sunlight. Limited by the characteristics of the material, the transmittance of the holographic material does not increase indefinitely but gradually tends to a certain value. The light transmittance data under different conditions are shown in Table III. The transmittance of the glass substrate and the recorded single-layer holographic film are 90% and 88% measured by a light transmittance meter. Experiments show that the transmittance of the HUD system has increased from 56% to 60% after being placed in the sun for a month.

C. Color Display

The monochromatic multi-plane display can satisfy the AR requirements in the vehicle display field. However, considering the driver's actual viewing comfort [24], it is better to display color images in each depth plane. Therefore, we propose two possible solutions to achieve multi-plane color display of different information.

Solution 1 is to divide the image source and HOEs into different areas. HOE_1 and HOE_2 are recorded in different areas of the holographic material. At the same time, the image source also needs to be divided into different areas in the same

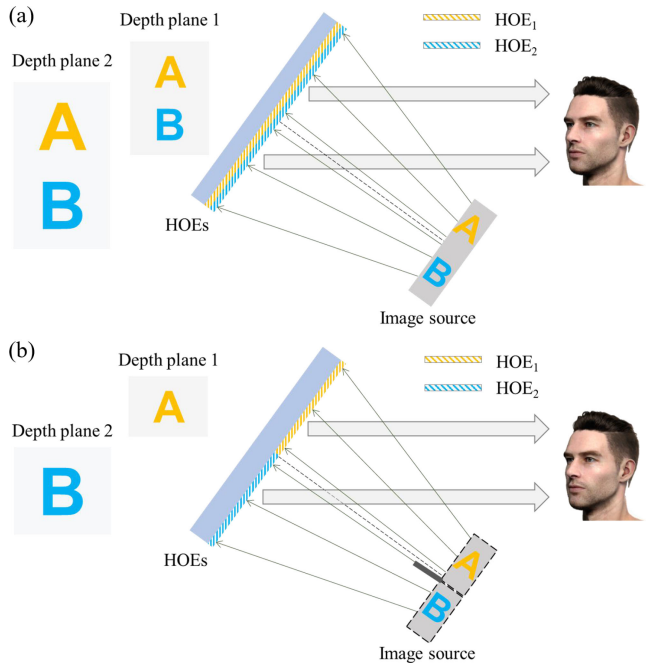

Fig. 12. (a) The imaging diagram when HOEs are not divided into multiple areas. The two depth planes display the same color information, and there is crosstalk between HOEs. (b) The imaging diagram when HOEs are divided into multiple areas. The two depth planes display different color information, and there is no crosstalk between HOEs.

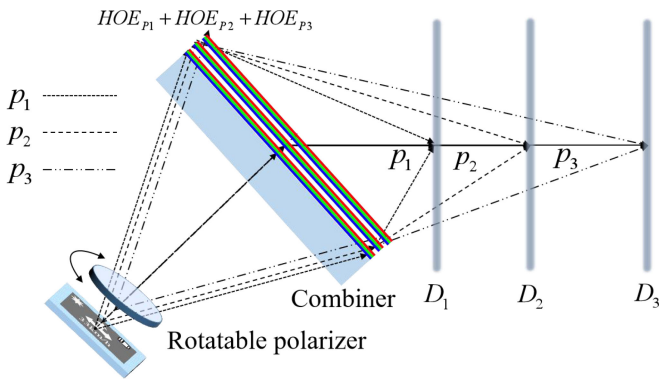

Fig. 13. A color multi-plane AR head-up display system based on polarization holographic optics.

form. Different color information will be diffracted by different HOEs and imaged on different depth planes. Fig. 12 shows the comparison of imaging diagrams before and after dividing HOEs into multiple areas.

Solution 2 is to use polarized volume grating (PVG) as the imaging element. Unlike VHG, as a kind of HOEs, PVG has a larger response bandwidth and has Pacharatnam-Berry (PB) phase polarization response characteristics [25]–[27]. The schematic diagram of this solution is shown in Fig. 13. First, a rotatable polarizer is added between the image source and the PVGs. The color signal light waves corresponding to the different polarization directions P_1, P_2, and P_3 of the different depth planes D_1, D_2, and D_3 can be obtained through the synchronization control and real-time refresh of the image source and the polarizer. Then, the color image of each depth plane is diffracted into the human eye by the color PVGs with corresponding polarization selectivity. And the holographic recording materials are required to have excellent polarization selection characteristics. In this system, the imaging optical elements are composed of three groups of HOEs with different polarization selectivity. And each group of PVGs is composed of red, green and blue gratings with the same polarization selectivity.

D. From C-Type HUD to W-Type HUD

Unlike the combiner-type (c-type) HUD, the windshield-type (w-type) holographic HUD requires a curved HOE because the windshield has curvature. The principle of the traditional w-type HUD is a transflective windshield based on geometric optics. Continental Corp. has proposed a HUD system that directly uses the windshield as a curved half mirror. However, the transflective HUD has the problems of low energy utilization, low design freedom, and large volume. The HUD based on HOEs can reduce the system volume, so it has huge potential application value. Wayray Corp. has demonstrated a HUD system using a curved HOE on the windshield, effectively reducing the size of the projection module. South Korea's Byoungho Lee *et al.* have proposed an analysis and design method for curved holographic optical elements, mainly analyzing the aberrations of two different recording methods: curved surface HOE and bendable surface HOE [21]. This method can effectively solve the aberration problem of the curved HOE. The Facebook reality laboratory research has proposed a design and fabrication method for freeform holographic optical elements [28]. This method has better design freedom, and can use optimization algorithms to correct the aberration of the curved HOE based on holographic printing. Therefore, we can further expand the w-type holographic HUD based on the large amount of work of the above-mentioned research teams in the future.

VI. Conclusion

We propose an AR HUD system with multi-plane, large area, high diffraction efficiency and a single PGU. Based on the angular selectivity and wavelength selectivity of the volume HOEs, HOEs of different wavelengths display images of different depths. We analyze and design the entire system theoretically, and perform numerical simulation and experimental verification. The integrated prototype is composed of a miniature laser projector, a scattering screen and three-layer HOEs. The red, green and blue HOEs are stacked on the same glass substrate with a thickness of 2 mm by vacuum bonding. Therefore, the diffraction efficiency of the system is maximized while ensuring lightness and thinness. The diffraction efficiencies of the red, green and blue HOEs measured in the experiment are 75.2%, 73.1% and 67.5%. The HOEs of red, green and blue respectively display images with depths of 150 cm, 500 cm and 1000 cm. The FOV and EB of the system are 12° × 10° and 9.5 cm × 11.2 cm. And the size of HOEs is 20 cm × 15 cm. In addition, the transmittance of the system has reached 60%. It is expected

that the proposed method will be widely used in augmented reality navigation display, such as vehicles, aviation, etc.

ACKNOWLEDGMENT

The authors thank the anonymous reviewers for their valuable suggestions.

REFERENCES

[1] T. Sasaki *et al.*, "Novel depth perception controllable method of WARP under real space condition," in *Proc. SID Symp. Dig. Tech.*, Oxford, U.K., 2011, pp. 244–267.

[2] G. Pettitt *et al.*, "47.1: Invited paper: Practical application of TI DLP technology in the next generation head-up display system," in *Proc. SID Symp. Dig. Tech.*, San Jose, CA, USA, 2015, pp. 700–703.

[3] J.-W. Lee *et al.*, "Development of lane-level guidance service in vehicle augmented reality system," in *Proc. Int. Conf. Adv. Commun. Technol.*, PyeongChang, Korea, 2015, pp. 263–266.

[4] J. A. Betancur *et al.*, "Research topics and implementation trends on automotive head-up display systems," *Int. J. Interactive Des. Manuf.*, vol. 12, no. 1, pp. 199–214, Feb. 2018.

[5] Z. Qin, F.-C. Lin, Y.-P. Huang, and H.-P. D. Shieh, "Maximal acceptable ghost images for designing a legible windshield-type vehicle head-up display," *IEEE Photon. J.*, vol. 9, no. 6, Dec. 2017, Art. no. 7000812.

[6] J. Nakagawa *et al.*, "Head up display with laser scanning unit," in *Proc. Ind. Opt. Devices Syst.*, San Diego, CA, USA, 2019, Art. no. 111250C.

[7] J. H. Seo *et al.*, "59-4: A study on multi-depth head-up display," in *Proc. SID Symp. Dig. Tech.*, LA, USA, 2017, pp. 883–885.

[8] Z. Qin *et al.*, "Dual-focal-plane augmented reality head-up display using a single picture generation unit and a single freeform mirror," *Appl. Opt.*, vol. 58, no. 20, pp. 5366–5374, Jul. 2019.

[9] H. S. Chen *et al.*, "Electrically adjustable location of a projected image in augmented reality via a liquid-crystal lens," *Opt. Exp.*, vol. 23, no. 22, pp. 28154–28162, Nov. 2015.

[10] T. Zhan *et al.*, "Pancharatnam-Berry optical elements for head-up and near-eye displays," *J. Opt. Soc. Amer. B*, vol. 36, no. 5, pp. D52–D65, May. 2019.

[11] S. Liu *et al.*, "51-3: A multi-plane optical see-through head mounted display with reverse mode PSLC," in *Proc. SID Symp. Dig. Tech.*, LA, USA, 2017, pp. 763–766.

[12] J. Kim *et al.*, "Foveated AR: Dynamically-foveated augmented reality display," *ACM Trans. Graph.*, vol. 38, no. 4, pp. 1–15, Jul. 2019.

[13] G. Xue *et al.*, "Multiplexing encoding method for full-color dynamic 3D holographic display," *Opt. Exp.*, vol. 22, no. 15, pp. 18473–18482, Jul. 2014.

[14] K. Wakunami *et al.*, "Projection-type see-through holographic three-dimensional display," *Nature Commun.*, vol. 7, no. 1, pp. 1–7, Oct. 2016.

[15] J. Christmas *et al.*, "75-2: Invited paper: Realizing auto-motive holographic head up displays," in *Proc. SID Symp. Dig. Tech.*, San Francisco, CA, USA, 2016, pp. 1017–1020.

[16] C. Mu *et al.*, "Zoomable head-up display with the integration of holographic and geometrical imaging," *Opt. Exp.*, vol. 28, no. 24, pp. 35716–35723, Nov. 2018.

[17] S. Q. Li *et al.*, "Phase-only transmissive spatial light modulator based on tunable dielectric metasurface," *Science*, vol. 364, no. 6445, pp. 1087–1090, Jun. 2019.

[18] P. Coni *et al.*, "56-1: A multiplane holographic HUD using light selectivity of bragg grating," in *Proc. SID Symp. Dig. Tech.*, San Jose, CA, USA, 2019, pp. 775–778.

[19] C. T. Draper *et al.*, "Holographic waveguide head-up display with 2-D pupil expansion and longitudinal image magnification," *Appl. Opt.*, vol. 58, no. 5, pp. A251–A257, Feb. 2019.

[20] S. Lee, B. Lee, J. Cho, C. Jang, J. Kim, and B. Lee, "Analysis and implementation of hologram lenses for see-through head-mounted display," *IEEE Photon. Technol. Lett.*, vol. 29, no. 1, pp. 82–85, Jan. 2017.

[21] K. Bang *et al.*, "Curved holographic optical elements and applications for curved see-through displays," *J. Inf. Display*, vol. 20, no. 1, pp. 9–23, Feb. 2019.

[22] H. Kogelnik, "Coupled wave theory for thick hologram gratings," *Bell Syst. Tech. J.*, vol. 48, no. 9, pp. 2909–2947, Nov. 1969.

[23] Z. Lv *et al.*, "Integrated holographic waveguide display system with a common optical path for visible and infrared light," *Opt. Exp.*, vol. 26, no. 25, pp. 32802–33281, Dec. 2018.

[24] S. A. Cholewiak *et al.*, "Chromablur: Rendering chromatic eye aberration improves accommodation and realism," *ACM Trans. Graph.*, vol. 36, no. 6, pp. 1–12, Nov. 2017.

[25] Y. H. Lee *et al.*, "Reflective polarization volume gratings for high efficiency waveguide-coupling augmented reality displays," *Opt. Exp.*, vol. 25, no. 22, pp. 27008–27014, Oct. 2017.

[26] Y. Weng *et al.*, "Liquid-crystal-based polarization volume grating applied for full-color waveguide displays," *Opt. Lett.*, vol. 43, no. 23, pp. 5773–5776, Dec. 2018.

[27] R. Chen *et al.*, "Multistimuli-responsive self-organized liquid crystal Bragg gratings," *Adv. Opt. Mater.*, vol. 7, no. 9, Feb. 2019, Art. no. 1900101.

[28] C. Jang *et al.*, "Design and fabrication of freeform holographic optical elements," *ACM Trans. Graph.*, vol. 39, no. 6, pp. 1–15, Nov. 2020.